INTERNATIONAL JOURNAL FOR NUMERICAL METHODS IN FLUIDS, VOL. 14, 1367–1376 (1992)

# A NEW DECOUPLED FINITE ELEMENT ALGORITHM FOR VISCOELASTIC FLOW. PART 1: NUMERICAL ALGORITHM AND SAMPLE RESULTS

S. J. SWARBRICK

*NNC Limited, Booths Hall, Knutsford, Cheshire WA16 9QZ, U.K.*

AND

V. NASSEHI*

*Department of Chemical Engineering, Loughborough University of Technology, Loughborough, Leicestershire, LE11 3TU, U.K.*

## SUMMARY

This paper presents an algorithm for two-dimensional steady viscoelastic flow simulation in which the solution of the momentum and continuity equations is decoupled from that of the constitutive equations. The governing equations are discretized by the finite element method, with $3 \times 3$ element subdivision for the stress field approximation. Non-consistent streamline upwinding is also used. Results are given for flow through a converging channel and through an abrupt planar 4:1 contraction.

KEY WORDS Finite elements Viscoelastic flow Convergence failure

## 1. INTRODUCTION

In recent years a number of attempts have been made to simulate viscoelastic flow by finite element discretization of the differential governing equations. Two particularly notable papers are those of Marchal and Crochet[1] and Luo and Tanner.[2] Marchal and Crochet used a coupled method in which the discretized governing equations are solved simultaneously for the full set of unknown variables (velocity, pressure and stresses). They employed a Newton iteration scheme. Element subdivision was used for the stress approximations and non-consistent streamline upwinding[3] was used to stabilize the iterative scheme. Consistent streamline upwinding[3] was found to be ineffective in this regard.

Luo and Tanner[2] used a decoupled method in which the solution of the flow equations (momentum conservation and continuity) is separated from that of the constitutive equations. The constitutive equations are thus solved with a fixed flow field, while the elastic extra stress appears as a pseudo-body force term in the momentum equations. Luo and Tanner used non-consistent streamline upwinding but did not use element subdivision.

Luo and Tanner found that convergence failure occurred for Weissenberg number ($We$) values greater than unity in the 4:1 contraction problem. With $4 \times 4$ element subdivision Marchal and

* Author to whom correspondence should be addressed.

0271–2091/92/111367–10$05.00
© 1992 by John Wiley & Sons, Ltd.
*Received May 1991*
*Revised November 1991*

Crochet found no indication of convergence failure in the 4:1 contraction problem with the Oldroyd-B model.[1,2]

In view of these results it is of interest to investigate the use of element subdivision in the decoupled method. Such a scheme is developed in this paper: $3 \times 3$ element subdivision is used for the stress approximations and non-consistent streamline upwinding is also used.

## 2. GOVERNING EQUATIONS

The governing equations employed are those of steady incompressible creeping flow of upper-convected Maxwell (UCM) and Oldroyd-B fluids in two dimensions.[1,2] Body forces are neglected. These assumptions regarding the nature of the flow are reasonable in the context of polymer-processing operations, although there is evidence to suggest that the restriction to two-dimensional flow and/or steady flow may be connected with the convergence failure of iterative solution schemes. This evidence is discussed by Brown *et al.*[4] and Lawler *et al.*[5] among others.

The governing equations in dimensionless form are

$$\nabla p - r\nabla \cdot (\nabla \mathbf{u} + \nabla \mathbf{u}^{\mathrm{T}}) = \nabla \cdot \mathbf{T}, \tag{1}$$

$$\mathbf{T} + De\overset{\nabla}{\mathbf{T}} = (1-r)(\nabla \mathbf{u} + \nabla \mathbf{u}^{\mathrm{T}}), \tag{2}$$

$$\nabla \cdot \mathbf{u} = 0, \tag{3}$$

where $p$ is pressure, $\mathbf{u}$ is velocity and $\mathbf{T}$ is the Maxwell extra stress tensor. $\overset{\nabla}{\mathbf{T}}$ is the upper-convected derivative of $\mathbf{T}$, defined by

$$\overset{\nabla}{T}_{ij} = \frac{\partial T_{ij}}{\partial t} + u_m \frac{\partial T_{ij}}{\partial x_m} - \frac{\partial u_i}{\partial x_m} T_{mj} - \frac{\partial u_j}{\partial x_m} T_{im}, \tag{4}$$

where $i, j, m = 1, 2$; $(x_1, x_2)$ denotes rectangular Cartesian co-ordinates and summation on repeated indices is assumed. $De$ is the Deborah number defined by $De = \lambda U/L$, where $U$ and $L$ are respectively a characteristic velocity and length for the flow and $\lambda$ is the relaxation time of the fluid (i.e. the characteristic time for the fluid to return to its initial state after a sudden deformation is imposed). The symbol '$r$' denotes the viscosity ratio, defined by $r = \eta_s/(\eta_s + \eta_m)$, where $\eta_m$ is the viscosity of the UCM fluid and $\eta_s$ is the viscosity of the Newtonian 'solvent'. The UCM governing equations are obtained by putting $r = 0$, while the Oldroyd-B case is given by $r = 0{\cdot}11$. The relation between Deborah number ($De$) and Weissenberg number ($We$) is given in Section 6.

As explained by Luo and Tanner,[2] the decoupled method requires a change of variable in the governing equations (1) and (2); this is to ensure that the discrete momentum equations always contain the real viscous term required to recover the Newtonian velocity–pressure formulation when $De$ approaches zero. The extra stress $\mathbf{T}$ is decomposed as

$$\mathbf{T} = \mathbf{S} + \mathbf{R}, \tag{5}$$

where

$$\mathbf{R} = (1-r)(\nabla \mathbf{u} + \nabla \mathbf{u}^{\mathrm{T}}). \tag{6}$$

In terms of $\mathbf{S}$ and $\mathbf{R}$ equations (1) and (2) become

$$\nabla p - \nabla \cdot (\nabla \mathbf{u} + \nabla \mathbf{u}^{\mathrm{T}}) = \nabla \cdot \mathbf{S}, \tag{7}$$

$$\mathbf{S} + De\overset{\nabla}{\mathbf{S}} = -De\overset{\nabla}{\mathbf{R}}. \tag{8}$$

Equations (3) and (6)–(8) are the governing equations used in the decoupled algorithm.

## 3. FINITE ELEMENT DISCRETIZATION

A weak variational statement of the problem based on a weighted residual representation of the governing equations is obtained and the resulting functionals are discretized using finite element interpolation. The weighted residual statement of equation (7) is

$$\int_\Omega [\nabla p - \nabla\cdot(\nabla\mathbf{u}+\nabla\mathbf{u}^{\mathrm{T}})]N\,\mathrm{d}\Omega = \int_\Omega (\nabla\cdot\mathbf{S})N\,\mathrm{d}\Omega, \tag{9}$$

where $N$ is a weighting function and $\Omega$ is the problem domain. The integrand on the LHS of equation (9) involves second-order derivatives of velocity. The velocity field is to be represented by quadratic interpolation functions, so in order to preserve interelement continuity, it is necessary to use Green's theorem in equation (9). This gives

$$\int_\Omega [(\nabla p)N + (\nabla\mathbf{u}+\nabla\mathbf{u}^{\mathrm{T}})\cdot\nabla N]\,\mathrm{d}\Omega = \int_\Omega (\nabla\cdot\mathbf{S})N\,\mathrm{d}\Omega + \int_\Gamma (\nabla\mathbf{u}+\nabla\mathbf{u}^{\mathrm{T}})\cdot\mathbf{n}N\,\mathrm{d}\Gamma, \tag{10}$$

where $\mathbf{n}$ is the unit outward normal to the boundary $\Gamma$.

The weighted residual statements of equations (3) and (8) are

$$\int_\Omega (\nabla\cdot\mathbf{u})N\,\mathrm{d}\Omega = 0, \tag{11}$$

$$\int_\Omega (\mathbf{S} + De\overset{\nabla}{\mathbf{S}})N\,\mathrm{d}\Omega = -\int_\Omega De\overset{\nabla}{\mathbf{R}}N\,\mathrm{d}\Omega. \tag{12}$$

The unknown variables are approximated using finite element interpolation functions. Velocity is approximated using nine-noded biquadratic elements, while pressure is approximated using the corresponding bilinear elements. The stresses are approximated using bilinear subelements obtained by $3\times 3$ subdivision of the velocity–pressure elements. The approximate forms of $\mathbf{u}$, $p$ and $\mathbf{T}$ on element '$e$' are given by

$$\mathbf{u}^e = \sum_I \mathbf{u}_I N_I, \qquad p^e = \sum_K p_K M_K, \qquad \mathbf{T}^e = \sum_L \mathbf{T}_L \mathbf{M}_L, \tag{13}$$

where $N_I$ and $M_K$ are biquadratic and bilinear shape functions respectively. The suffices $I$, $K$ and $L$ label the nodes of the respective elements.

A Galerkin approximation to the weighted residual equations is now obtained by using the approximate forms (13). The biquadratic and bilinear basis functions are also used as weighting functions. The momentum and continuity equations give rise to a $22\times 22$ elemental stiffness matrix which may be represented as follows:

$$\begin{bmatrix} \int_{\Omega_e}(2N_{I,1}N_{J,1}+N_{I,2}N_{J,2})\,\mathrm{d}\Omega & \int_{\Omega_e} N_{I,2}N_{J,1}\,\mathrm{d}\Omega & \int_{\Omega_e} N_I M_{K,1}\,\mathrm{d}\Omega \\ \int_{\Omega_e} N_{I,1}N_{J,2}\,\mathrm{d}\Omega & \int_{\Omega_e}(N_{I,1}N_{J,1}+2N_{I,2}N_{J,2})\,\mathrm{d}\Omega & \int_{\Omega_e} N_I M_{K,2}\,\mathrm{d}\Omega \\ \int_{\Omega_e} M_L N_{J,1}\,\mathrm{d}\Omega & \int_{\Omega_e} M_L N_{J,2}\,\mathrm{d}\Omega & 0 \end{bmatrix} \begin{bmatrix} U_J^1 \\ U_J^2 \\ P_K \end{bmatrix} = \begin{bmatrix} \int_{\Omega_e} S_{1j,j}N_I\,\mathrm{d}\Omega + \int_{\Gamma_e} d_{1j}n_j N_I\,\mathrm{d}\Gamma \\ \int_{\Omega_e} S_{2j,j}N_I\,\mathrm{d}\Omega + \int_{\Gamma_e} d_{2j}n_j N_I\,\mathrm{d}\Gamma \\ 0 \end{bmatrix}. \tag{14}$$

In equation (14) the subscripts $I$ and $J$ label the nine nodes of the biquadratic element, while $K$ and $L$ label the four nodes of the bilinear element. Partial differentiation with respect to $x(y)$ is

denoted by subscript ',1' (subscript ',2'). The $j$th velocity components at node $J$ is denoted by $u_J^j$. Summation on repeated indices is assumed. The $N_I$ and $M_L$ are the weighting functions. The first two lines of the matrix correspond to the two components of the vector equation (10), while the third line corresponds to equation (11). The components of the tensor $(\nabla \mathbf{u} + \nabla \mathbf{u}^T)$ are denoted by $d_{ij}$. The domain of integration for element '$e$' is denoted by $\Omega_e$, while $\Gamma_e$ denotes the boundary of element '$e$'.

Isoparametric mapping is used to express the integrands in equation (14) in terms of local element co-ordinates[6] and the integrals are then evaluated by Gaussian quadrature. The resulting elemental matrices and load vectors are then assembled and a frontal elimination/back-substitution routine[6] is used to solve the resulting system for the nodal unknowns $u_J^i$ and $P_K$.

In each iterative loop the stress fields are computed after the velocity field. The viscous stress **R** (equation (6)) is obtained by 'variational recovery'. This means that equation (6) is represented in Galerkin weighted residual form and the resulting system is solved for the nodal values of **R**. The elastic stress **S** is then computed using a Galerkin approximation to equation (12). The corresponding elemental stiffness equation may be represented as follows:

$$\begin{bmatrix} \int M_I M_J \, d\Omega + De \int u^m M_I^* M_{J,m} \, d\Omega - 2De \int u^1_{,1} M_I M_J \, d\Omega & 0 & 2De \int u^1_{,2} M_I M_J \, d\Omega \\ 0 & \int M_I M_J \, d\Omega + De \int u^m M_I^* M_{J,m} \, d\Omega - 2De \int u^2_{,2} M_I M_J \, d\Omega & 2De \int u^2_{,1} M_I M_J \, d\Omega \\ -De \int u^2_{,1} M_I M_J \, d\Omega & -De \int u^1_{,2} M_I M_J \, d\Omega & \int M_I M_J \, d\Omega + De \int u^m M_I^* M_{J,m} \, d\Omega + De \int u^1_{,1} M_I M_J \, d\Omega + De \int u^2_{,2} M_I M_J \, d\Omega \end{bmatrix} \begin{bmatrix} S_J^{11} \\ S_J^{22} \\ S_J^{12} \end{bmatrix} = \begin{bmatrix} De \int \bar{R}^{11} M_I \, d\Omega \\ De \int \bar{R}^{22} M_I \, d\Omega \\ De \int \bar{R}^{12} M_I \, d\Omega \end{bmatrix} \tag{15}$$

Non-consistent streamline upwinding, applied to the convective terms only, has been used in equation (15). The upwinded weighting functions are indicated by asterisks. They are given by, for element '$e$',

$$M_I^* = M_I + \frac{\phi h^e}{|\mathbf{u}|} \mathbf{u} \cdot \nabla M_I, \tag{16}$$

where $|\mathbf{u}|$ is the magnitude of $\mathbf{u}$, $h^e$ is the element size function and $\phi$ is a scaling factor. This technique has the effect of smoothing the oscillations which occur when the standard Galerkin method is used to solve convection-dominated equations. The element size function is given by $h^e = \sqrt{[(x_{,\xi} + x_{,\eta})^2 + (y_{,\xi} + y_{,\eta})^2]}$, where $(\xi, \eta)$ are the element local co-ordinates.

The elemental equations (15) are assembled and solved in the same manner as for equations (14).

## 4. BOUNDARY CONDITIONS

Some consideration must be given to the boundary integrals in equation (14). When the global matrix is assembled, the boundary integrals for all elemental boundary segments in the interior of the problem domain sum to zero. On the global domain boundary, two essential boundary condition values are given at each node, except for nodes which lie on the outlet part of the boundary or on an axis of symmetry (if there is one). In the assembled global stiffness matrix, any row corresponding to a degree of freedom for which an essential boundary constraint is specified will be eliminated in the solver routine.

At each outlet node, one essential boundary constraint is given, namely zero velocity parallel to the boundary. For the normal direction a natural boundary condition must be given. The boundary integrand for the normal direction contains the factor $d_{1j}n_j$, i.e. the normal component of viscous traction. This may be set to zero, which is equivalent to assuming fully developed flow for a viscous fluid. In each flow domain which we consider, the outlet is placed at the end of a straight extension channel, so the assumption of fully developed flow is reasonable.

At each node on a symmetry axis, zero normal velocity component is given, so the natural boundary condition in this case is zero viscous traction parallel to the axis.

## 5. SOLUTION ALGORITHM

The iterations start from the Newtonian creeping flow field obtained by solving the discrete forms of equations (3) and (7) with $\mathbf{S}=0$. The basic algorithm is as follows.

Step 1. Read in Newtonian flow field.
Step 2. Compute viscous stress field **R** (equation (6)).
Step 3. Compute elastic stress field **S** (equation (8)).
Step 4. Compute new flow field **u**, $p$ (equation (7)).

Repeat steps 2–4 until the solution converges.

## 6. SAMPLE RESULTS

Two test problems which have been investigated using the algorithm described above are (i) flow through a 30° planar converging half-channel and (ii) flow through a planar abrupt 4:1 contraction. These domains are of interest since they involve both shear and extensional flow and provide stringent tests of the algorithm.

*Converging channel*

Three meshes have been used for this problem. Figures 1(a)–1(c) show the $3 \times 3$ subelement meshes used for the stress approximations. Mesh 1 has 612 elements, with 68 elements in the corresponding velocity–pressure meshes. Meshes 2 and 3 each have 918 elements, with 102 elements in the corresponding velocity–pressure meshes. The inlet is at the wider end. The boundary conditions are as follows.

(a) Wall boundary: no slip.
(b) Flow axis: zero normal velocity, zero shear stress.
(c) Inlet: zero tangential velocity, imposed normal velocity profile, imposed stresses.
(d) Outlet: zero tangential velocity, natural boundary condition (zero normal viscous traction).

Some convergence limits are shown in Table I. The values quoted are those of the Weissenberg number defined by $We = \lambda \dot{\gamma}_w$, where $\dot{\gamma}_w$ is the wall velocity gradient at the outlet. In the upwinded cases the value $\phi = 1$ is used for the upwinding scale factor.

The use of the non-consistent streamline upwinding improves the performance of the iterative scheme, as does the use of Oldroyd-B rather than the UCM model. It was also found that the use of the SUPG formulation[1,2] (i.e. consistent upwinding) did not improve the performance. In both

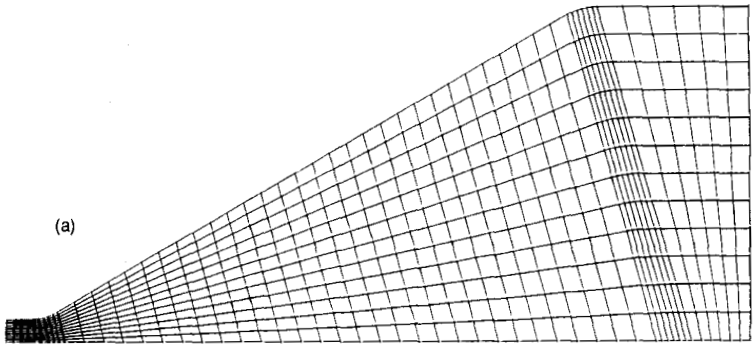


Figure 1(a). Mesh 1 (converging channel)

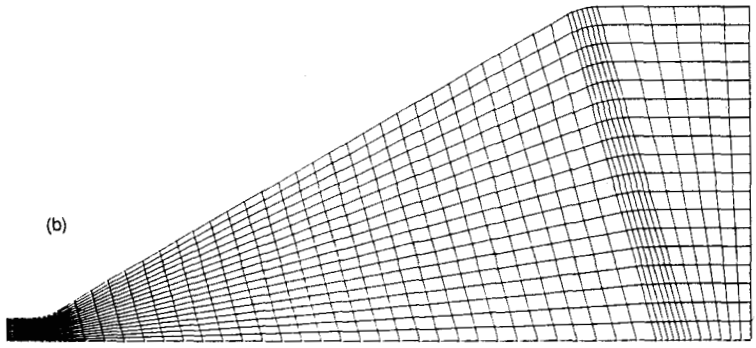


Figure 1(b). Mesh 2 (converging channel)

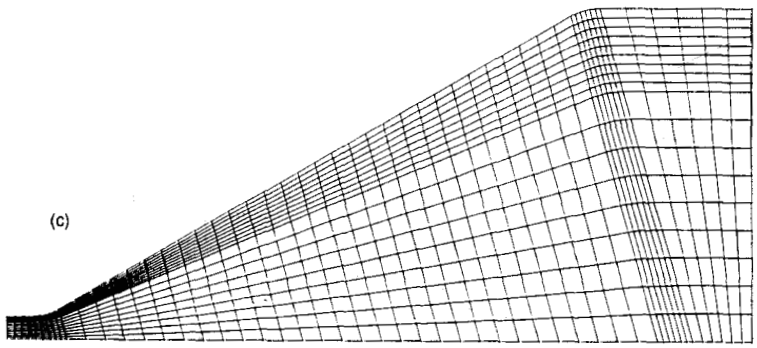


Figure 1(c). Mesh 3 (converging channel)

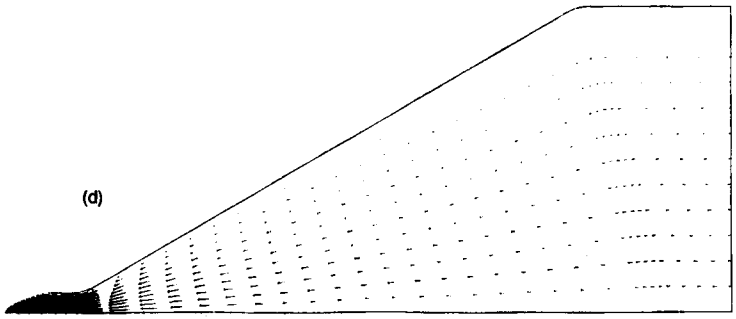


Figure 1(d). Velocity vectors for converging channel: UCM case at $We = 1{\cdot}6$

Table I. Convergence limits for converging channel

| | Mesh 1 | Mesh 2 | Mesh 3 |
|---|---|---|---|
| UCM, upwinded | 2·6 | 2·2 | 2·4 |
| Oldroyd-B, not upwinded | 1·6 | | |
| Oldroyd-B, upwinded | 3·3 | | |

the converging channel and 4:1 contraction problems, loss of convergence was associated with the loss of positive definiteness of the matrix

$$\mathbf{T}_A = \mathbf{T} + \frac{(1-r)\mathbf{I}}{De},$$

where $\mathbf{I}$ is the unit matrix. All these findings are consistent with those of References 1 and 2.

The convergence limits are lower for the more refined meshes 2 and 3 than they are for mesh 1. It was also found that higher convergence limits were obtained if element subdivision was not used for the stress representation. However, in that case the stress representation is much cruder than it is when element subdivision is used. The stress fields develop much larger gradients than do the velocity fields and so a more refined mesh is required to approximate them. The use of element subdivision permits this while minimizing the consequent increase in computational cost (since larger elements are still used for the velocity field).

Note that mesh 3 gives a higher convergence limit than mesh 2; the design of mesh 3 permits a more accurate representation of the stress gradient close to the wall boundary.

Figure 1(d) shows an example of the velocity field obtained in the converging channel. This is as expected. As the convergence limit is approached, the instability of the numerical solution is less apparent in the velocity field than it is in the stress fields.

Figure 2 shows the significant normal stress component $T^{11}$ plotted across the outlet for mesh 2 at $We = 1{\cdot}6$. ($T^{22}$ is very small at the outlet).

The non-upwinded Oldroyd-B case (circles) gives a higher gradient near the wall than the upwinded case (triangles), while the upwinded UCM case (squares) gives a gradient lying between these two. This result is consistent with the convergence limits for the three cases given in Table I (under mesh 1). It is also consistent with the suggestion that one of the causes of convergence failure may be the inability of the element discretization to resolve steep stress gradients (as discussed in Reference 4).

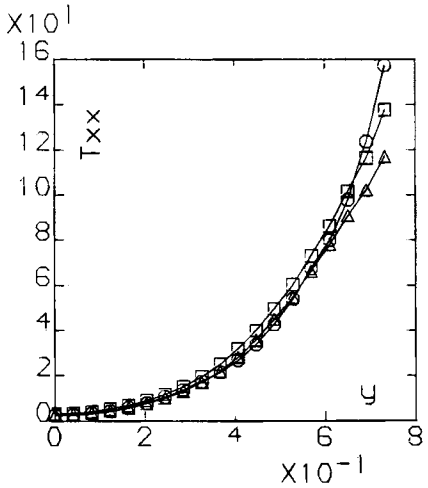


Figure 2. Plots of $T^{11}$ for converging channel mesh 2 at $We = 1{\cdot}6$, taken across the outlet; circles, Oldroyd-B, not upwinded; triangles; Oldroyd-B, upwinded; squares; UCM, upwinded

(a)

Figure 3(a). Mesh 1 (4:1 contraction)

(b)

Figure 3(b). Mesh 2 (4:1 contraction)

(c)

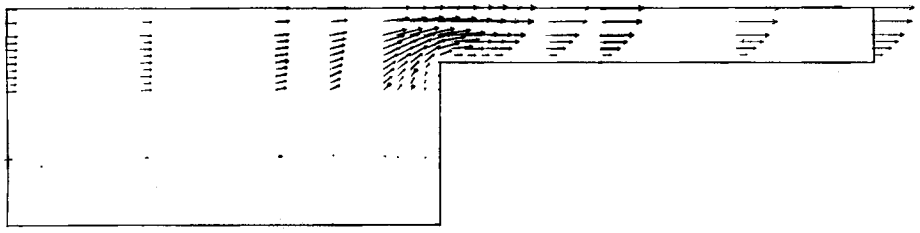

Figure 3(c). Velocity vectors for 4:1 contraction: UCM case at $We = 1$

*Abrupt 4:1 contraction*

Two meshes have been used for this problem and are shown in Figures 3(a) and 3(b). As before, the $3 \times 3$ subelement meshes are shown. Mesh 1 has 324 elements, corresponding to 36 velocity–pressure elements; mesh 2 has 405 elements, corresponding to 45 velocity–pressure elements. Boundary conditions are the same as for the converging channel problem.

Table II. Convergence limits for 4:1 contraction

| | Mesh 1 | Mesh 2 |
|---|---|---|
| UCM | 1·7 | 1·6 |
| Oldroyd-B | 1·75 | |

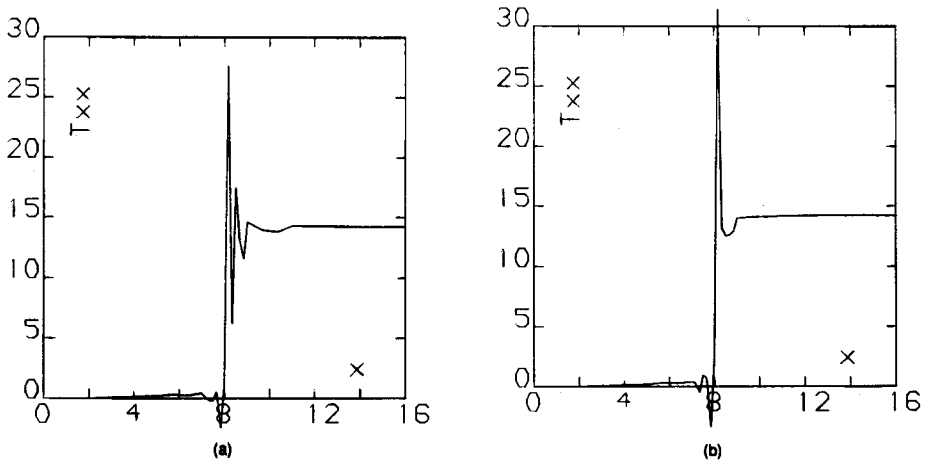


Figure 4. Plots of $T^{11}$ for 4:1 contraction mesh 2 at $We=1$, taken from inlet to outlet through the re-entrant corner (at $x=8$): (a) Oldroyd-B, not upwinded; (b) Oldroyd-B, upwinded

Some convergence limits are shown in Table II. Non-consistent streamline upwinding (with $\phi=1$) was used in each case. The limits shown here are lower than those of Reference 2, when convergence up to $We=5{\cdot}5$ was obtained for the planar 4:1 contraction with the Oldroyd-B model. This may be because the velocity–pressure mesh used here is too coarse to accurately represent the steep pressure gradients at the re-entrant corner.

Figure 3(c) shows a typical velocity field for the 4:1 contraction; again this is as expected. Figures 4(a) and 4(b) show plots of $T^{11}$ taken along the length of the channel from the inlet ($x=0$) to the outlet ($x=16$) and passing through the re-entrant corner ($x=8$). These plots correspond to the sample solutions obtained for $We=1$. Figures 4(a) and 4(b) are for the Oldroyd-B cases without and with upwinding respectively. The smoothing effect of the non-consistent streamline upwinding is clearly seen.

## 7. CONCLUSIONS

A decoupled finite element algorithm for steady two-dimensional flow simulation in viscoelastic fluids has been developed which incorporates subelement representation for the stress fields and non-consistent streamline upwinding. The algorithm has been tested in the context of the converging channel and 4:1 contraction problems and convergence has been obtained for values of $We$ greater than unity.

The algorithm could be particularly useful as a basis for further developments. In view of the results reported in References 1 and 2, it would be of interest to investigate the use of higher levels of mesh refinement and of element subdivision arrangements other than those used so far.

## REFERENCES

1. J. M. Marchal and M. J. Crochet, 'A new mixed finite element for calculating viscoelastic flow', *J. Non-Newtonian Fluid Mech.*, **20**, 77–114 (1987).
2. X. L. Luo and R. I. Tanner, 'A decoupled finite element streamline-upwind scheme for viscoelastic flow problems', *J. Non-Newtonian Fluid Mech.*, **31**, 143–162 (1989).
3. A. N. Brooks and T. J. R. Hughes, 'Streamline-upwind/Petrov Galerkin formulations for convection dominated flows with particular emphasis on the incompressible Navier–Stokes equations', *Comput. Methods Appl. Mech. Eng.*, **32**, 199–259 (1982).
4. R. A. Brown, R. C. Armstrong, A. N. Beris and P. W. Yeh, 'Galerkin finite element analysis of complex viscoelastic flows', *Comput. Methods Appl. Mech. Eng.*, **58**, 201–226 (1986).
5. J. V. Lawler, S. J. Muller, R. A. Brown and R. C. Armstrong, 'Laser Doppler velocimetry measurements of *velocity* fields and transitions in viscoelastic fluids', *J. Non-Newtonian Fluid Mech.*, **20**, 51–92 (1986).
6. O. C. Zienkiewicz and K. Morgan, *Finite Elements and Approximation*, Wiley, New York, 1983.